Alt, J.C., Kinoshita, H., Stokking, L.B., and Michael, P.J. (Eds.), 1996
Proceedings of the Ocean Drilling Program, Scientific Results, Vol. 148

21. ELECTRICAL CONDUCTION IN OCEANIC DIKES, HOLE 504B[1]

André Revil,[2] Michel Darot,[2] Philippe A. Pezard,[3] and Keir Becker[4]

ABSTRACT

Porosity, cation-exchange capacity (CEC), and electrical conductivity have been measured on 28 doleritic minicores from Deep Sea Drilling Project (DSDP) and Ocean Drilling Program (ODP) Hole 504B (Legs 137, 140, and 148). Conductivity experiments were performed under five different saturating-fluid salinities, at room temperature and pressure, and with a two-electrode conducting cell. At 4 kHz, the porosity is related to the "intrinsic" formation factor by an inverse power law similar to Archie's formula $F = a\,\phi^{-m}$ with $m = 0.94$ and $a = 16$ for the fine-grained specimens. Such a low m value suggests a current conduction in cracks and microcracks present at mineral scale throughout the rock. The presence of clays as alteration products is reflected by the high values of CEC. As expected, Q_V/F (where Q_V is the CEC per unit pore volume) and the surface conductivity are well correlated. This point leads to an estimate of the surface tortuosity. The temperature dependence of the surface conductivity is extracted using data on DC electrical conductivity at different temperature. For temperature correction purposes, a linear temperature dependence appears to be a good estimate for this parameter.

On the basis of these results, an equation was given that allows estimation of the porosity from resistivity measurements in Hole 504B. This equation was tested by comparing the predicted conductivity against the measured conductivity of a large set of samples.

INTRODUCTION

This work continues a series of studies (Pezard and Anderson, 1989; Pezard et al., 1989; Pezard, 1990) aimed at understanding the transport properties (hydraulic and electrical conductivities) in the upper art of the oceanic crust. This paper is primarily concerned with the measurement of electrical conductivity of doleritic samples from Ocean Drilling Program (ODP) Hole 504B, where a 1-km dike complex was drilled. In this environment, rocks are saturated with hot hydrothermal solutions under pressure. The electrical properties of rocks depend strongly on microstructural and thermodynamical parameters. For example, the chemistry and salinity of the saturating brine and the geometry of the void (cracks and pores) network are controlling parameters together with pressure and temperature (Duba et al., 1988). In the holes drilled in the upper part of the oceanic crust, the formation water in the vicinity of the borehole is supposed to be seawater (Mottl et al., 1983), and the influence of temperature and salinity on sodium chloride aqueous solutions is well known (Sen and Goode, 1992).

Early works on electrical properties of oceanic rocks were published by Hyndman (1974), and Drury (1976). Complementary to these studies, the present paper shows the drastic effect of surface conductivity on electrical conductivity of dolerite samples. In particular, the temperature dependence of surface conductivity is twice as large as the temperature dependence of fluid conductivity. The aim of this paper is to derive a relation between the electrical conductivity and the porosity for dolerites which accounts for previously observed effects.

In the first part of this paper, we determined the in-phase electrical conductivity of 28 samples of dolerite at 4 kHz. Archie's formula parameters and surface tortuosity were also determined. On the basis of these results, we derived and tested a relation linking the electrical conductivity to porosity, bulk tortuosity, and cation-exchange capacity (CEC).

In the second part of this paper, the electrical conductivity of 12 samples was measured as a function of temperature. An apparatus was designed for conducting measurements on saturated samples in the temperature range 20°–90°C. These measurements were performed with five different fluid salinities at room pressure with a two-electrode conducting cell. We investigated the influence of temperature on both the surface conductivity (resulting from the double layer at the interface between the matrix and pore space) and the formation factor. These results allowed us to incorporate the temperature correction in the relation found at the end of the first section.

DC CONDUCTIVITY

The following measurements of DC electrical conductivity and microstructure parameters were obtained at laboratory temperature.

Core Measurements

Measurements were performed on 28 doleritic minicores from the dikes of Hole 504B, sampled between 1575 and 1926 m below seafloor (mbsf). The samples were cut from the working halves of the cores, perpendicular to the axis of the original core. The samples were cylinders, 25.4 mm in diameter (except for six samples from Leg 148, which were 18.9 mm in diameter) and 17 to 29 mm in length. Before this study, the samples were stored in seawater to prevent desaturation. Proper care was taken to obtain parallel specimen faces. The 28 samples were grouped into three categories by visual examination: type I (fine-grained specimens), type II (medium-grained specimens), and type III (medium-grained, bluish greenish gray matrix specimens).

[1] Alt, J.C., Kinoshita, H., Stokking, L.B., and Michael, P.J. (Eds.), 1996. *Proc. ODP, Sci. Results,* 148: College Station, TX (Ocean Drilling Program).

[2] Ecole et Observatoire de Physique du Globe de Strasbourg, 5 rue René Descartes, F-67084 Strasbourg Cedex, France. Revil: andre@climont.u-strasb.fr

[3] Laboratoire de Mesures en Forage, Institut Méditerranéen de Technologie, Technopôle de Château-Gombert, F-13451 Marseille Cedex 20, France; and Laboratoire de Pétrologie Magmatique, URA CNRS 1277, Faculté des Sciences et Techniques de Saint-Jérôme, Avenue Escadrille Normandie-Niemen, F-13397 Marseille Cedex 20, France. pezard@imtmer1.imt-mrs.fr

[4] Marine Geology and Geophysics, Rosenstiel School of Marine and Atmospheric Sciences, 4600 Rickenbacker Causeway, University of Miami, Miami, FL 33149-1098, U.S.A. kbecker@rsmas.miami.edu

According to core descriptions (Shipboard Scientific Party, 1992a, 1992b, 1993), the sample textures are as follows: Type I = very fine grained (Section 137-504B-174R-1 and Sections 137-504B-180M-1 and 180M-2) or microcrystalline to fine-grained aphanitic for all others; Type II = either seriate porphyritic (Section 140-504B-200R-3) or medium-grained doleritic for all others; Type III = more complicated texture, but all samples are subophitic. Type III occurs in the deepest samples from Hole 504B (Sections 140-504B-227R-2 through 227R-11) and in all samples from Leg 148.

The connected porosity and the matrix density were measured on the 28 samples of dolerite using the triple-weighing method. After being evacuated, plugs were kept for four days in distilled water to saturate. Dry mass was measured after drying the samples at 70°C for 2 hr. A drying test was performed on a few samples for 10 hr: no significant variation was found. The experimental error was less than 15% for connected porosity (ϕ) and less than 2% for matrix density (ρ_m).

The CEC parameter accounts for the number of counter-ions that might contribute to the surface conduction. A standard technique of measuring CEC in rocks is the Kjeldahl method described by Ridge (1983). This method is a chemical analysis. A cation not native to the rock is first fixed on the exchangeable clay sites, then the fixed cations are removed and their amount measured. A small volume of each sample was crushed for these measurements. Laboratory data are summarized in Table 1. These values are converted into CEC per unit pore volume $Q_V^{(c)}$ in the following way (Clavier et al., 1977):

$$Q_V^{(c)} = \rho_m \frac{1-\phi}{\phi} CEC_{(c)}, \qquad (1)$$

where the superscript (c) means that this parameter is deduced from chemical measurements. We will develop this point further.

Electrical conductivity was measured along the axis of the samples, and is thus representative of the "horizontal" conductivity of the bulk rock. Measurements were made using stainless-steel electrodes applied against sample ends. To avoid possible spurious contact potentials between electrodes and conductive minerals, filter-paper disks (soaked in the brine) were placed between the sample ends and the electrodes. Despite this precaution, the overall error was as high as 5% because of the difficulty in achieving a reproducible contact between the sample and the electrodes (the instrumental error itself was on the order of 1%). Electrode polarization occurred below 1 kHz, which is why a frequency of 4 kHz was chosen to measure the sample conductivity σ.

Specimens were evacuated before saturation with degassed NaCl brines. The concentrations used (0.0095, 0.10, 0.64, 1.45, and 2.12 M), correspond respectively to the fluid conductivities at room temperature and pressure (0.1, 1, 5, 10, and 14 S/m). The samples were stored in the saturating solution for at least 5 days before the measurements were made and the solution was checked for salinity stability. After the measurements were completed, several samples were re-equilibrated at various salinities; typically the value of σ was repeatable to 4% or better. Furthermore, electrical conductivity was measured on dry rock to check matrix conductivity, it was found to be negligible compared with total conductivity.

Results

The results of the physical and chemical measurements are summarized in Table 1. The porosity of the medium-grained samples (type II) is 0.6% ± 0.1%; for fine-grained samples (type I), porosity ranges between 0.2% and 1.8% (note the large scatter in this case). For type III samples, porosity is between 0.2% and 1.3%. Matrix density for types I and II is 2.95 ± 0.05 g/cm^3, whereas type III (deeper) samples have a slightly lower mean density (2.87 ± 0.04 g/cm^3). The cross-plot diagram of matrix density vs. electrical resistivity at seawater salinity (Fig. 1) exhibits peculiar clustering corresponding to the three sample types. Therefore, texture and electrical resistivity

Table 1. Results of physical and chemical measurements.

Core, section, interval (cm)	Type	Depth (mbsf)	σ_S	F	ϕ	ρ_m	$CEC_{(c)}$	$Q_V^{(c)}$	$\sigma(\sigma_w)$ 0.1	1	5	10	14
137-504B-													
174R-1, 96	I	1577.3	8.5	1530	0.53	2.97	1.8	0.97	2.2	9.49	41.2	73.7	100.0
174R-1, 115	I	1577.5	2.7	1880	0.72	2.92	2.0	0.78	2.6	8.12	30.2	53.8	78.3
180M-1, 93	I	1619.3	2.9	4390	0.33	2.97	1.8	1.56	1.2	3.31	14.3	25.5	34.8
180M-2, 100	I	1620.9	3.6	4490	0.25	2.98	—	—	1.6	4.48	15.0	25.3	35.1
140-504B-													
186R-1, 79	I	1627.1	1.8	1810	1.76	2.92	—	—	2.4	7.20	28.5	59.5	78.1
186R-2, 35	I	1628.1	1.9	2480	1.84	2.91	2.1	0.31	3.4	7.31	22.4	41.5	58.8
186R-2, 43	I	1628.2	4.2	2880	0.97	2.93	—	—	2.0	5.32	21.7	39.0	53.0
200R-3, 14	II	1731.7	8.0	880	0.52	2.96	—	—	2.1	12.00	63.7	124.6	165.9
200R-3, 118	II	1732.8	10.3	830	0.76	2.94	3.1	1.15	3.3	14.67	71.1.	129.5	179.6
204R-1, 51	I	1757.0	6.7	1780	0.62	2.92	3.0	1.36	2.7	6.60	35.1	62.6	85.8
205R-1, 27	I	1757.3	2.8	4320	0.97	2.93	2.8	0.81	1.9	4.53	14.2	26.2	35.0
208R-2, 100	II	1780.5	7.8	1250	0.70	2.95	2.3	0.93	3.0	11.95	48.0	87.0	119.9
210R-1, 19	II	1795.1	5.9	650	0.71	2.98	1.4	0.56	3.0	16.64	83.1	157.6	221.1
210R-1, 117	II	1796.1	13.4	550	0.84	2.96	2.9	0.98	4.4	21.29	102.6	196.2	264.7
225R-1, 28	I	1912.5	3.9	2540	0.63	2.96	1.6	0.72	1.3	5.01	24.9	40.5	60.7
225R-1, 48	I	1912.7	1.9	2250	0.58	2.95	0.8	0.39	1.3	5.21	24.2	46.1	64.2
225R-1, 138	II	1913.6	8.5	820	0.69	2.97	—	—	4.1	14.36	68.5	132.8	178.0
225R-2, 09	II	1913.8	6.5	640	0.61	2.98	—	—	2.4	15.97	83.8	163.6	223.9
225R-2, 43	II	1914.1	4.5	830	0.61	2.97	—	—	2.1	12.90	63.8	128.6	172.5
226R-1, 62	II	1920.6	11.2	950	0.73	2.94	2.5	0.96	3.0	15.88	63.0	118.0	157.4
226R-2, 130	II	1922.8	7.9	680	0.75	2.95	1.6	0.60	3.5	17.17	80.3	157.5	212.3
227R-2, 11	III	1926.0	1.2	1250	3.32	2.82	1.6	0.13	4.4	9.6	40.6	82.0	112.2
148-504B-													
240R-1, 82	III	2007.7	3.8	677	0.54	2.87	—	—	4.1	20.4	74.5	153	—
241R-1, 26	III	2016.8	4.7	1201	0.69	2.89	—	—	3.5	14.4	43.9	89	—
241R-1, 56	III	2017.1	—	350	1.33	2.91	—	—	4.5	25.1	121.5	269	—
249R-1, 138	III	2072.7	2.7	791	1.01	2.86	—	—	4.0	16.7	61.4	130	—
251R-1, 23	III	2090.1	4.4	1128	0.33	2.90	—	—	3.3	13.3	48.5	93	—
251R-1, 47	III	2090.4	0.9	863	0.23	2.92	—	—	3.4	12.9	58.0	117	—

Notes: Type I = fine-grained specimens, type II = medium-grained specimens, and type III = medium-grained specimens with bluish greenish gray matrix. All conductivity values are given in 10^{-4} S/m. σ_S = surface conductivity, F = formation factor, ϕ = porosity (in %), ρ_m = matrix density (in g/cm^3), $CEC_{(c)}$ = chemical cation-exchange capacity, and σ = rock conductivity at various concentrations yielding fluid conductivities σ_w, at 20°C, of 0.1, 1, 5, 10, and 14 S/m. $Q_V^{(c)}$ (in 10^9 Cb/m^3) is the counter-ion density per unit of pore volume and is estimated from the chemical CEC using Equation 1. Dashes (—) indicate samples not measured.

appear well correlated in our samples; the medium-grained samples are the most conductive whereas the fine-grained samples are the most resistive.

The full expression for the sample conductivity is the sum of two terms: bulk conductivity and surface conductivity (Waxman and Smits, 1968; Clavier et al., 1977; Kulenkampff and Schopper, 1988; Johnson and Schwartz, 1989). If volume conduction and surface conduction are in parallel, the sample conductivity can be written as

$$\sigma = \frac{1}{F}\sigma_w + \sigma_S, \tag{2}$$

where σ_S is the surface conductivity resulting from the electric double layer on the internal surface (Ucok, 1979; Clavier et al., 1977). F, the formation factor of the rock, is an intrinsic property of the porous medium that depends upon its texture (i.e., the distribution of pore and crack sizes, their aspect ratios, arrangement, connectivity, and flow-path tortuosity). In Equation 2, the rock conductivity is a linear function of the fluid conductivity.

As demonstrated rigorously by Johnson and Sen (1988), Equation 2 is valid for high-concentration electrolytes (or "high salinities" according to Johnson and Sen) and results from a much more complex expression. Actually, the convexity of the σ vs. σ_w plot (Waxman and Smits, 1968; Clavier et al., 1977) can be explained by the different tortuosities between surface and volume conduction paths (Johnson and Sen, 1988). As σ_w increases, dominant current paths shift from surface to pore and therefore are subjected to different tortuosities.

The plot of σ (sample conductivity at 4 kHz) vs. σ_w shows a linear relationship where the fluid conductivity is larger than 0.1 S/m, that is, 0.10 M for T = 20°C (Fig. 2A). On this linear portion, the formation factor F and the surface conductivity are, respectively, the slope inverse and the σ-axis intercept of the σ vs. σ_w curve. Another, more traditional use of this data is to plot the logarithm of the electrical conductivity of the saturated sample vs. the logarithm of the conductivity of the saturating electrolyte (Kulenkampff and Schopper, 1988; Pezard et al., 1989). At high salinities (in the approach of Pezard et al., 1989), most conduction occurs through the bulk solution and the second term of Equation 2 is negligible. In this case, the logarithm plot is a straight line of the unity gradient. At low salinities, the first term of Equation 2 becomes negligible and the rock conductivity tends to the constant value of surface conductivity (Fig. 2B). The only advantage of this last representation is the ability to see for a given electrolytic conductivity (for example, seawater conductivity at 5 S/m) which is the most important mechanism (i.e., pore volume or surface conductivity). It is interesting that these two equivalent representations do not give the same definition of high- and low-salinity domains. In the present work, low and high salinities will be referred to as in Pezard's work.

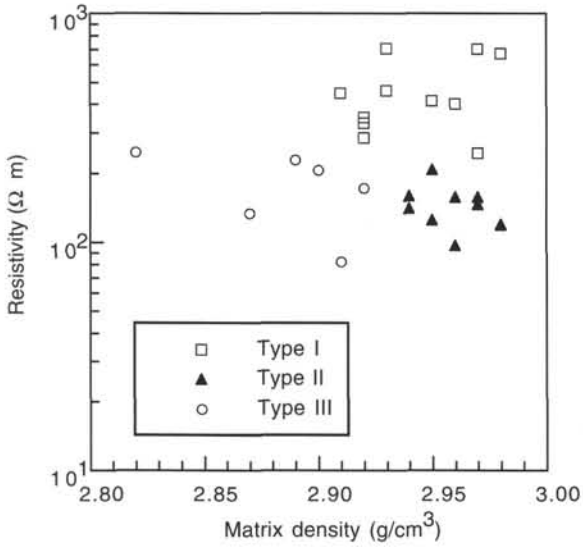

Figure 1. Resistivity (measured at seawater salinity, 5 S/m) vs. matrix mean density (ρ_m).

As stated previously, $Q_V^{(c)}$ is deduced from CEC chemical measurements using Equation 1. In Figure 3, $Q_V^{(c)}$ divided by the formation factor F is reported vs. surface conductivity σ_S. Because CEC chemical measurements are made on crushed samples, all electrical sites of the clays (i.e., charge default) are investigated. This explains the strong link between chemical CEC, $CEC_{(c)}$, and the clay percentage of a shaly rock (Waxman and Smits, 1968; Clavier et al., 1986). This is not the case for electrical conductivity measurements where only an effective fraction of clays participates in surface conduction. We will note this fraction as f_a. More precisely, f_a is the fraction of all interconnected clay sites that are responsible for surface conductivity, $0 \le f_a \le 1$. Actually, the meaning of "connected sites" follows the percolation theory: it refers to sites that are part of an "infinite path" (Gueguen and Dienes, 1989). With this definition, it is obvious that surface conductivity can be linked to the $Q_V^{(c)}$ parameter by

$$\sigma_S = \frac{\beta f_a Q_V^{(c)}}{F}, \tag{3}$$

where β is the equivalent conductance of the counter-ions absorbed onto the pore surfaces. A standard analytical model, used by Pape et al. (1985) for granite and Wilkens et al. (1989), and Pezard (1990) for oceanic basalts, represents the surface conductivity with

$$\sigma_S = \frac{\beta \cdot Q_V^{(c)}}{F\tau_S^2}, \tag{4}$$

where τ_S is a factor related to the tortuosity of pore surface (Pape et al., 1985). This parameter can be seen as the "excess of tortuosity of pore surface," thus, as the ratio of the mean current surface lines on the mean current lines of the pore volume. It should be remembered that measurements are studied in the "high-salinity domain" (as defined by Johnson and Sen, 1988), where surface and volume conduction are "in parallel." Consequently, $F_S = F\,\tau_S^2$ is the formation factor associated with the surface conduction and the lower limit for the surface tortuosity is 1. The volume tortuosity is defined by $F = \tau_V^2 / \phi$.

Comparison between Equations 3 and 4 involves $f_a \sim 1/\tau_S^2$. Indeed, this means that "the tortuosity concept that is used frequently in rock physics and the percolation concept are related" (Gueguen and Dienes, 1989). If a mean value of 2.5×10^{-8} m²/V/s is considered for the counter-ion mobility β (see the discussion for this parameter in Sen and Goode, 1992), then, knowing the surface conductivity and $Q_V^{(c)}$, one can estimate the square of the surface tortuosity. Linear regression on the data given in Figure 3 gives $\tau_S^2 \approx 21$ for type I and $\tau_S^2 \approx 31$ for type II (or $f_a \approx 5\%$ and $f_a \approx 2\%$, respectively). Such a value suggests a highly complicated pore surface for all samples from dikes.

The formation factor depends on porosity and tortuosity of the pore space (Carman, 1956). For a collection of similar samples, the connected porosity is related to the formation factor by the Winsauer and McCardell (1953) equation, which is better adapted to crystalline rocks than is Archie's formula (Pezard, 1990):

$$F = a\phi^{-m}, \tag{5}$$

where a and m are called by extension "Archie's parameters." The factor a can be seen as the mean volume tortuosity of the formation. For the fine-grained specimens, a linear regression (Fig. 4) yields $a \approx 16 \pm 2$ and $m \approx 0.94$. Pezard et al. (1989) showed that such a low m value indicates that the conducting pore space of doleritic rocks is composed mainly of cracks and microcracks. The range of porosity

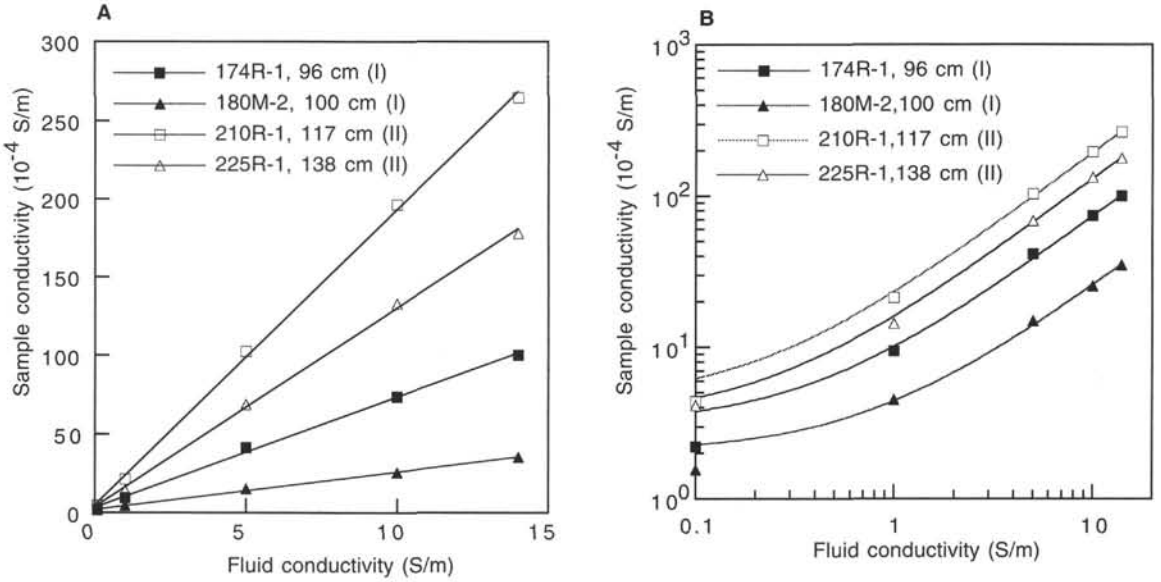

Figure 2. Sample conductivity vs. fluid conductivity.

for the medium-grained specimens (type II) is too narrow for these parameters to be determined. However, if m is assumed to equal 1, then $a \approx 5$ for this sample family.

In the future, the results of this study will be used to analyze the resistivity log obtained from Hole 504B to provide a way to estimate in situ porosity. During ODP Leg 148, the Schlumberger dual laterolog (DLL) tool (Serra, 1984; Ellis, 1987) was run over the entire length of the basement section in Hole 504B to measure the rock electrical resistivities surrounding the borehole. The frequency measurement of this tool is close to 100 Hz. A question arises whether the conductivity value σ at 4 kHz (the frequency used for laboratory measurements) is close to the DC conductivity σ_0 (i.e., evaluated at zero frequency) and can be compared to the value given by the DLL in situ. We have found experimentally that σ values are within 5% of the inverse of the DC resistivity values derived from the Argand plots ($\rho_0 = 1/\sigma_0$).

Another important point is to know if the contribution of the surface conductivity can be ignored in the dikes of Hole 504B. In the case of the upper oceanic crust drilled with seawater, borehole and pore fluids have similar salinities (Mottl et al., 1983). The mean ratio between the surface conductivity and the rock conductivity at seawater salinity is close to 10% (at room pressure and temperature). Because surface conductivity increases much faster than brine conductivity with temperature, the surface conductivity contribution can not be neglected in the dikes of Hole 504B because of the hole's elevated temperature (120°–160°C). The electrical conduction in the dike is consequently a combination of two mechanisms: electrolytic conduction within the pore space (i.e., fluid-filled cracks and pores), and surface conduction at pore-matrix interface.

Unlike bulk density, acoustic velocity, or electrical resistivity, porosity is not directly measurable in situ. Using observations and data from this study, the electrical conductivity of dikes samples can be written in term of porosity, bulk tortuosity, τ_V and total CEC. Taking $F = \tau_V^2/\phi$ and assuming $\phi << 1$, Equations 1 and 2 can be rewritten, which leads to the semi-empirical formula

$$\sigma = \frac{\phi}{\tau_V^2}\sigma_w + 2.8010^{-3}\frac{CEC_{(c)}}{\tau_V^2}. \quad (6)$$

Here $CEC_{(C)}$ is the cation-exchange capacity in meq/100 g. The numerical term in the surface conductivity was calculated with a matrix density of $\rho_m \approx 2.90$ g/cm^3, a counter-ion mobility $\beta = 2.5 \times 10^{-8}$ SI, and a surface tortuosity $\tau_S^2 = 25$. Equation 6 was tested with 48 experimental data points corresponding to samples of type I (except samples from Core 140-504B-186X) and type II and in the high salinity domain (0.64, 1.45, and 2.12 M). Type III samples were not used because of their large data scatter. The bulk tortuosity was taken to equal 13 for type I (fine-grained samples) and 5 for type II (medium-grained samples). Results are reported in Figure 5. Where CEC data were not available, a mean value of 2.1 meq/100 g was taken to compute the surface conductivity.

Equation 6 was used to determine the porosity from in situ resistivity measurements made in Hole 504B. In this case, the problem is the determination of the cation-exchange capacity in the formation. Scala (see Clavier et al., 1977) found a strong correlation between gamma-ray (GR) count rate divided by the porosity and Q_V. In other words, GR logging can be used as a direct measure of the CEC (and not Q_V), and the proportionality constant could be determined using the laboratory data and in situ measurements.

TEMPERATURE CORRECTION

Within deep holes in the oceanic crust, temperature varies with depth. To derive porosity from in situ resistivity measurements, the influence of this parameter must be taken into account. For that, we measured the temperature influence of electrical conduction parameters for 12 samples (four for each of the three types).

Experimental Procedure and Apparatus

The equipment used to measure temperature dependence consists of a series of cells mounted within a frame (Fig. 6). The holding screw ensures good electrical contact between the electrodes and the samples. The frame is immersed in a temperature-controlled bath. Measurements were performed over a temperature range between 20° and 90°C, in drained conditions to minimize geometrical effects (i.e., open pore circuit), because in the present paper we are not interested in studying the effect of thermal hydrocracking on rock electrical conductivity as shown by Llera et al. (1990). No hysteresis was found after a complete temperature cycle (i.e., no irreversible damage is induced during the test; Fig. 7). Reproducibility was also checked, and no significant effect was found.

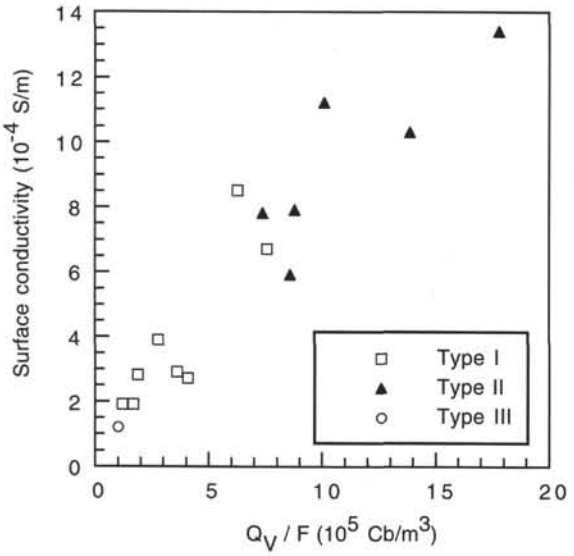

Figure 3. Surface conductivity plotted as a function of $Q_V^{(c)}/F$.

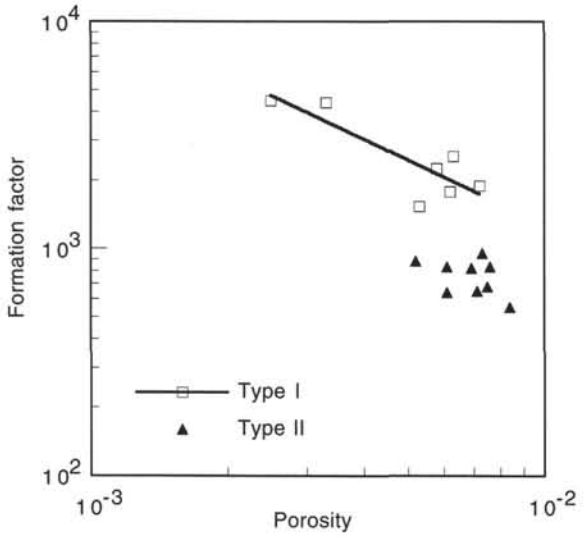

Figure 4. Formation factor vs. porosity.

Each conductivity cell was connected to a measuring circuit (a Schlumberger Solartron impedancemeter). Stainless-steel plates at the sample end act as both current and potential electrodes. All measurements were performed at 4 kHz to minimize the effects of polarization at the interfaces between the samples and electrodes. An insulating adhesive tape was used to avoid unacceptable leakage currents. This tape is heat resistant (to 105°C) and readily adheres to most rocks and minerals. Filter-paper disks were used to prevent contact polarization effects between the electrodes and the sample.

Using water as the heating liquid in the temperature-controlled bath it implies an upper boundary for the temperature near 90°–95°C. Each step in temperature takes 10 min. After testing the time needed to reach temperature equilibrium, a duration of 20 min was adopted to ensure uniform heating in each sample after each temperature step.

Sample Conductivity

In Figure 8, sample conductivity is plotted vs. temperature. Different brine concentrations were used (0.0095, 0.0500, 0.10, 0.35, and 0.64 M) for our experiments. As expected, the sample conductivity increases with the brine concentration and with the temperature. This increase is well described by a linear relationship, for which we introduce the coefficient α:

$$\alpha = \frac{1}{\sigma(T_0)}\left(\frac{\partial \sigma}{\partial T}\right)_P . \quad (7)$$

The subscript (P) indicates that we worked at constant fluid pressure because of the drained conditions. As the fluid conductivity decreases, dominant current paths shift from pore to surface. However, surface conductivity is much more temperature dependent than is bulk conductivity (see, e.g., Clavier et al., 1977). This result is

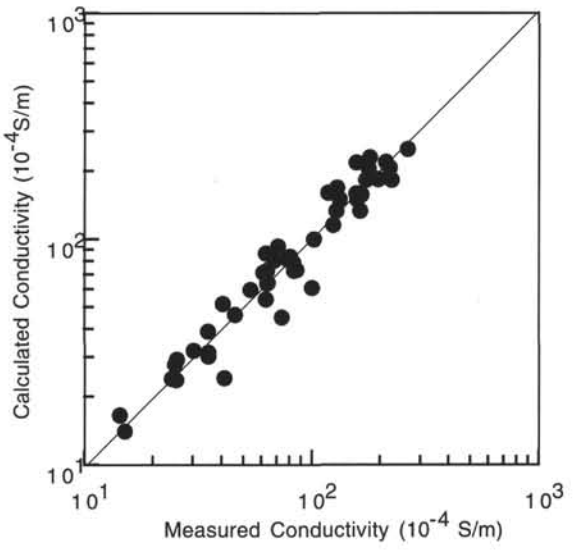

Figure 5. Comparison of conductivity calculated using Equation 6 with 48 experimental data points (types I and II only).

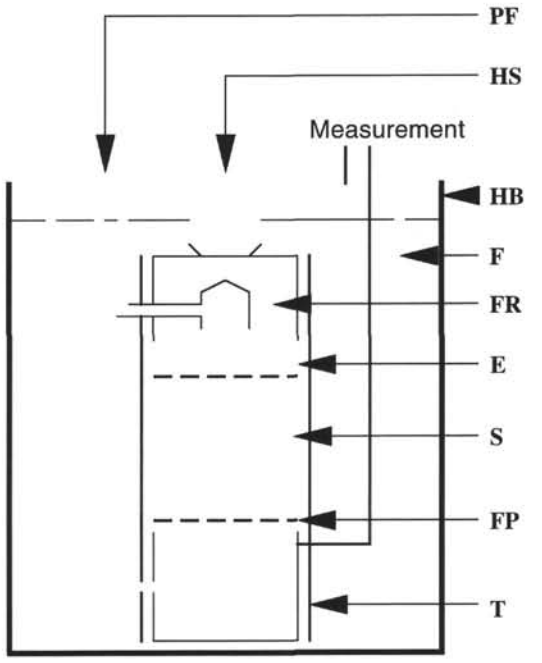

Figure 6. The conductivity cell. E = stainless-steel electrode, F = frame, FP = fluid pipe, FR = fluid reservoir (polycarbonate), HB = heating bath, HS = holding screw (to maintain electrical contacts during temperature exploration), PF = pore fluid, S = sample, and T = heat-resistant insulating tape.

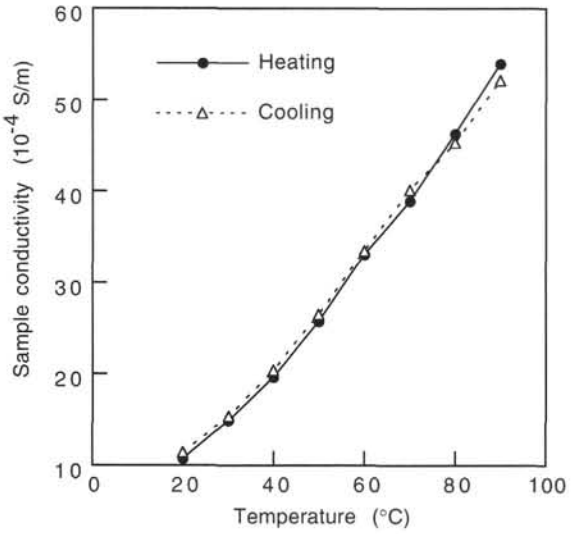

Figure 7. Hysteresis effect during a temperature cycle.

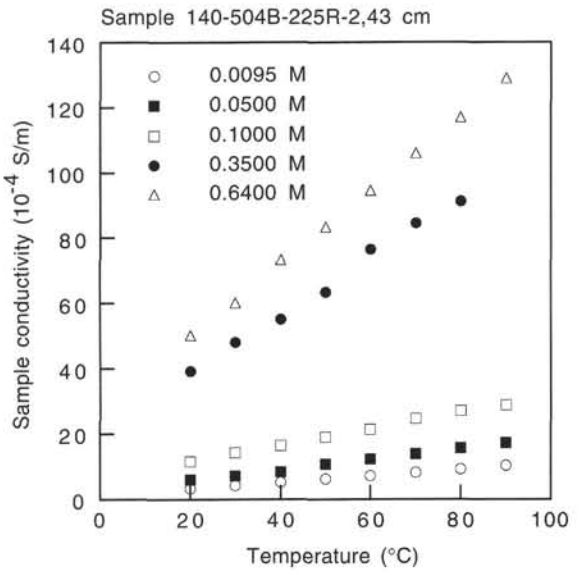

Figure 8. Temperature dependence of electrical conductivity for different molalities.

well observed in Figure 9, where α is plotted as a function of the brine concentration. At high salinities, α is close to the dependence coefficient of fluid conductivity (i.e., 0.023 SI, as shown in the next section); at low salinities, α increases.

Brine Conductivity

The conductivity of the NaCl aqueous solution used can be computed using the Sen and Goode (1992) semi-empirical formula:

$$\sigma_w = (5.6 + 0.27T - 1.510^{-4}T^2)M - \frac{2.36 + 0.099T}{1.0 + 0.214M}M^{3/2}, \quad (8)$$

where σ_w is in S/m[1], M is the molality, and T is the temperature (°C). This formula can be used over a temperature range 20°–200°C and over the molality range used in the present study. Equation 8 was tested with success in our laboratory. Thus, this equation allowed us to plot the sample conductivity vs. the brine conductivity for different temperatures.

If fluid expansion is neglected, all the temperature dependence of the brine conductivity is a result of the ion mobilities. Mobility can be defined by (see, for example, Llera et al., 1990)

$$\beta = \frac{Ze}{6\pi\eta_f r}, \quad (9)$$

where η_f is the fluid viscosity, e the electron charge, Z the ion valence, and r the effective radius of the ion, assumed to be a sphere. For simple ions, mobilities are typically on the order of 10^{-8} m²/V/s. As it is well known that the temperature dependence of η_f can be expressed by an exponential law (η_f decreases as temperature increases), the temperature dependence of ion mobility must follow a similar relation (i.e., the same activation energy). If the results are plotted on an Arrhenius diagram, data points should be well aligned and the mobility may be expressed by an exponential formula:

$$\beta_i(T) = \beta_i \exp\left(-\frac{E_a^{(S)}}{RT}\right), \quad (10)$$

where β_i is a constant independent of the temperature, $E_a^{(S)}$ is referred to as the thermal activation energy and may give an idea of the mechanisms of electrical conduction, and R is the international gas constant (R = 8.32 in SI units). However, for a simple system such as water, the activation energy of viscosity extracted from Equation 10 is temperature dependent (Sperkach and Shakhpanorov, 1981). In this case, the activation energy decreases from 16 kJ (at 25°C) to 10 kJ (at 200°C). As the fluid conductivity is linked to the mean mobility $\bar{\beta}_w$ by

$$\sigma_w = 10^3 \bar{\beta}_w MeN, \quad (11)$$

where N is the Avogadro number (6.023×10^{23}/mol), the temperature dependence of $\beta_w(T)/\beta_w(T_0)$ can be computed from Equation 8 for different molalities (Fig. 10). This plot shows that the temperature dependence can be well described by a linear relation in a temperature range of 20°–200°C. Thus, it is possible to write

$$\sigma_w(M,T) = \sigma(M,T_0)[1 + \alpha_w(T - T_0)], \quad (12)$$

where α_w is less sensitive to M and T. For an NaCl brine, α_w is close to 0.0230 ± 0.001 SI for the salinity range investigated. As stated in the previous section, in the high-salinity domain the value of α is close to this value of α_w.

Formation Factor and Surface Conductivity

The temperature dependence of rock electrical conductivity for shaly rocks is a function of the temperature dependence of bulk and surface conductivities (Ohloeft, 1981; Pezard, 1990; Sen and Goode, 1992) and electrolyte conductivity. Data points are well aligned on a σ vs. σ_w diagram for high σ_w (i.e., high salinities). Then, from a linear regression, it is possible to derive the formation factor as the slope inverse of σ vs. σ_w for different temperatures. In Figure 11, formation factor is reported vs. temperature for several samples. The small variations on the variation of formation factor with temperature up to 90°C do not indicate any particular trend. This implies that no significant physical change in pore structure occurs within this temperature range because the formation factor remains constant as long as the porosity is unchanged (see Eq. 5). The work of Ucok (1979) confirmed this result on a temperature range 20°–175°C. Beyond 175°C, the apparent increase in formation factor is a sign of changes in the structure of core samples as a result of thermal expansion. Johnston (1987) showed for three shale samples a dependence of the formation factor with the temperature in a range of 20°–100°C, but shales have a special microstructure that could explain this temperature dependence.

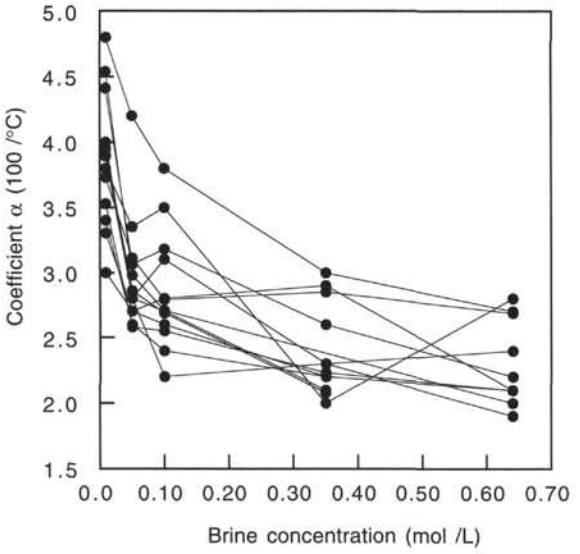

Figure 9. Coefficient α vs. brine concentration.

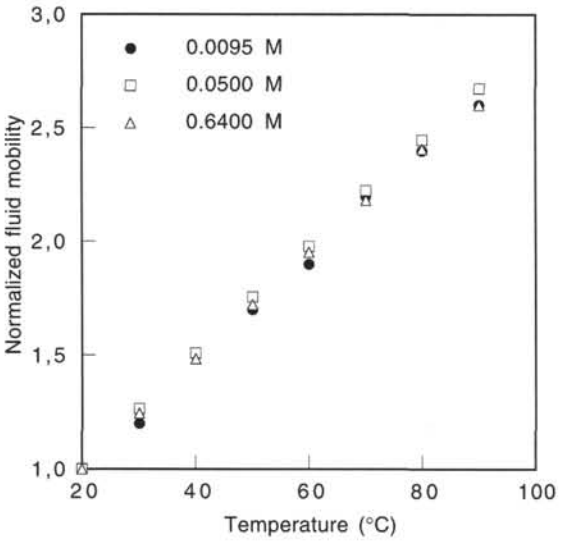

Figure 10. Normalized fluid mobility vs. temperature.

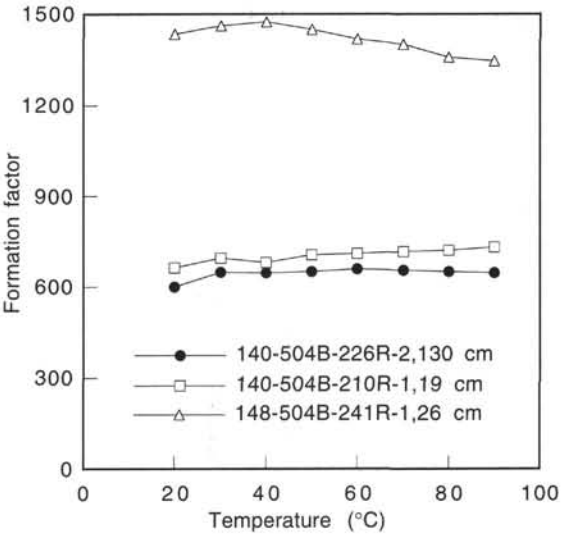

Figure 11. Formation factor vs. temperature.

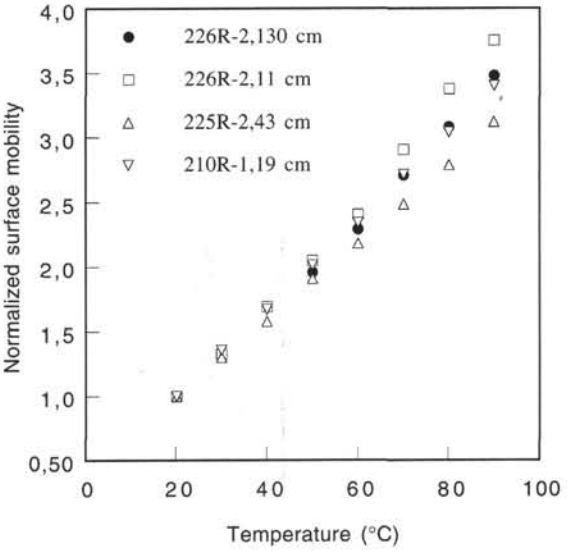

Figure 12. Normalized surface mobility vs. temperature (type II samples).

After studying, the formation factor we investigated the influence of the temperature on surface conductivity. To compute the surface conductivity as a function of temperature, we used the low salinity data set. For constant-charge clay surfaces, the surface conductivity may be roughly estimated by Equation 4. Clay minerals (except zeolites, Yariv and Cross, 1979; Olhoeft, 1981; Talibudeen, 1981) have surfaces with constant charges (and therefore are of constant CEC). In the absence of significant pore-volume deformation as a result of a temperature increase, the temperature dependence of the surface conductivity is attributable to the counter-ion mobility, β. In this case, the temperature dependence on this parameter is computed using

$$\frac{\beta(T)}{\beta(T_0)} = \frac{F(T)\sigma(T) - \sigma_w(T)}{F(T_0)\sigma(T_0) - \sigma_w(T_0)}. \qquad (13)$$

For example, for each sample of type II the temperature dependence of the counter-ion mobility results are reported in Figure 12. A least-squares fit to these data yields

$$\beta(T) = \beta(T_0)[1 + \alpha_S(T - T_0)], \qquad (14)$$

with $\alpha_S = 0.045/°C \pm 0.005/°C$ for type I, $0.037/°C \pm 0.003/°C$ for type II, and $0.039/°C \pm 0.009/°C$ for type III. Similarly, for the large temperature range of 20°–200°C, Clavier et al. (1977) and Sen and Goode (1992) used a linear temperature dependence for the counter-ion mobility of shaly sands saturated with an NaCl electrolyte with $\alpha_S = 0.0328/°C$ for Clavier and $\alpha_S = 0.0414/°C$ for Sen and Goode.

Discussion

A question arises whether the conductivity value can be predicted for in situ temperature (i.e., 130°–170°C) by the extrapolation of low-temperature data (i.e., 20°–90°C) from this study. Previous works such as Ucok (1979), for a large variety of rock types (including basalt samples), show that this extrapolation is possible for temperatures below 200°C. Actually, the resistivity of rock samples saturated with NaCl solution exhibits a sharp decrease with temperature near

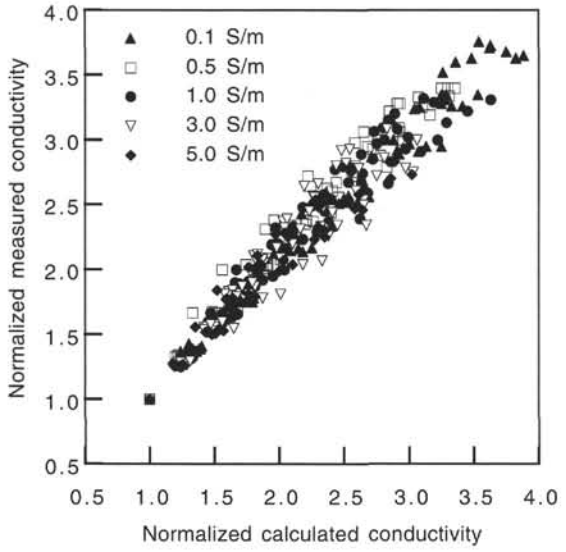

Figure 13. Comparison of conductivity calculated using Equation 15 with 433 experimental data points (types I, II, and III). Calculated and measured values are normalized to values at 20°C for each salinity value.

200°C and the rate of decrease in resistivity decreases considerably beyond this temperature.

Laboratory data shed some light on possible conduction mechanisms as a function of salinity and temperature. Therefore, the relative importance of the two conduction mechanisms active in the upper oceanic crust during in situ resistivity experiments can be estimated and the porosity can be derived. This is made possible by incorporating the temperature dependence of both surface and bulk conductivity in Equation 6:

$$\sigma(M,T) = \frac{\phi}{\tau_V^2}\sigma_w(M,T) + 2.80\ 10^{-3}\frac{CEC_{(c)}}{\tau_V^2}\frac{\beta(T)}{\beta(T_0)}, \qquad (15)$$

where $\sigma_w(M, T)$ is given by Equation 8 at seawater salinity (approximately 0.64 M) and $\beta(T)/\beta(T_0)$ is given by Equation 13, with T_0 = 20°C and $\alpha_S = 0.040$°C. In Figure 13, we test this equation with success by considering values of τ_V, ϕ, and *CEC* for each sample.

CONCLUSIONS

Our work shows that electrical DC resistivity can be used to group doleritic rocks into three species: fine and medium-grained specimens of doleritic samples from Legs 137 and 140 (except for Sample 140-504B-227R-2, 11 cm) and a third group that corresponds to deeper specimens from Hole 504B. The bulk tortuosity was estimated as 16 for type I (fine-grained) and 5 for type II (medium-grained) samples. The surface tortuosity estimated from chemical CEC measurements and surface conductivity equals 21 for type I samples and 31 for type II samples.

The temperature dependence of the sample conductivity follows a linear relationship. This linear dependence is expressed with the coefficient α, which decreases with brine concentration. The surface conductivity varies linearly with temperature, with the coefficient α_S close to 0.040/°C. The microgeometry of the pore space does noticeably change with temperature variation because, to a first approximation, the formation factor is constant.

Using these results, a semi-empirical formula, linking rock electrical conductivity to porosity, bulk tortuosity, and CEC was proposed and tested on a large data set. This equation is a potential tool for the derivation porosity from in situ measurements (resistivity and gamma ray).

ACKNOWLEDGMENTS

The authors thank A. Decarreau for the CEC measurements at Poitiers. We thank Dr. Y. Bernabe and Dr. C. David for helping to shape a better manuscript through informal discussions. M. Drury is also acknowledged for his review of the paper. This study was supported by CNRS URA 1358 and 1277.

REFERENCES

Carman, P.C., 1956. *Flow of Gases Through Porous Media:* San Diego (Academic).

Clavier, C., Coates, G., and Dumanoir, J., 1986. The theoretical and experimental basis for the "dual-water" model for the interpretation of shaly sands. *In* Schmidt, A. (Ed.), *Openhole Well Logging.* Soc. Pet. Eng., SPE Repr. Ser., 21:357–372.

Drury, M.J., 1976. Electrical resistivity of basalts, Leg 34. *In* Yeats, R.S., Hart, S.R., et al., *Init. Repts. DSDP,* 34: Washington (U.S. Govt. Printing Office), 549–552.

Duba, A., Huenges, E., Nover, G., Will, G., and Jödicke, H., 1988. Impedance of black shale from Münsterland 1 borehole: an anomalously good conductor? *Geophys. J.,* 94:413–419.

Ellis, D.V., 1987. *Well Logging For Earth Scientists:* New York (Elsevier).

Gueguen, Y., and Dienes, J., 1989. Transport properties of rocks from statistics and percolation. *Math. Geol.,* 21:1–13.

Hyndman, R.D., 1974. Electrical resistivity of basalts from DSDP Leg 26. *In* Davies, T.A., Luyendyk, B.P., et al., *Init. Repts. DSDP,* 26: Washington (U.S. Govt. Printing Office), 505–508.

Johnson, D.L., and Schwartz, L.M., 1989. Unified theory of geometrical effects in transport properties of porous media. *Log Analyst,* 30:98. (Abstract)

Johnson, D.L., and Sen, P.N., 1988. Dependence of the conductivity of a porous medium on electrolyte conductivity. *Phys. Rev. B,* 37:3502–3510.

Johnston, D.H., 1987. Physical properties of shale at temperature and pressure. *Geophysics,* 52:1391–1401.

Kulenkampff, J., and Schopper, J.R., 1988. Low frequency complex conductivity: a means for separating volume and interlayer conductivity. *Trans. 11th Eur. Form. Eval. Symp.,* Paper P.

Llera, K.J., Sato, M., Nakatsuka, K., and Yokoyama, H., 1990. Temperature dependence of the electrical resistivity of water-saturated rocks. *Geophysics,* 55:576–585.

Mottl, M.J., Anderson, R.N., Jenkins, W.J., and Lawrence, J.R., 1983. Chemistry of waters sampled from basaltic basement in Deep Sea Drilling Project Holes 501, 504B, and 505B. *In* Cann, J.R., Langseth, M.G., Honnorez, J., Von Herzen, R.P., White, S.M., et al., *Init. Repts. DSDP,* 69: Washington (U.S. Govt. Printing Office), 475–483.

Olhoeft, G.R., 1981. Electrical properties of rocks. *In* Touloukian, Y.S., Judd, W.R., and Roy, R.F. (Eds.), *Physical Properties of Rocks and Minerals:* New York (McGraw-Hill), 257–330.

Pape, H., Riepe, L., and Schopper, J.R., 1985. Petrophysical detection of microfissures in granites. *Trans. SPWLA 26th Annu. Logging Symp.,* P1–P17.

Pezard, P.A., 1990. Electrical properties of mid-ocean ridge basalt and implications for the structure of the upper oceanic crust in Hole 504B. *J. Geophys. Res.,* 95:9237–9264.

Pezard, P.A., and Anderson, R.N., 1989. Morphology and alteration of the upper oceanic crust from in-situ electrical experiments in DSDP/ODP Hole 504B. *In* Becker, K., Sakai, H., et al., *Proc. ODP, Sci. Results,* 111: College Station, TX (Ocean Drilling Program), 133–146.

Pezard, P.A., Howard, J.J., and Lovell, M.A., 1989. Clay conduction and pore structure of oceanic basalts from DSDP/ODP Hole 504B. *In* Becker, K., Sakai, H., et al., *Proc. ODP, Sci. Results,* 111: College Station, TX (Ocean Drilling Program), 97–108.

Ridge, M.J., 1983. A combustion method for measuring the cation-exchange capacity of clay minerals. *Log Analyst,* 3:6–11.

Sen, P.N., and Goode, P.A., 1992. Influence of temperature on electrical conductivity on shaly sands. *Geophysics,* 57:89–96.

Serra, O., 1984. *Fundamentals of Well-Log Interpretation* (Vol. 1): *The Acquisition of Logging Data:* New York (Elsevier).

Shipboard Scientific Party, 1992a. Site 504. *In* Becker, K., Foss, G., et al., *Proc. ODP, Init. Repts.,* 137: College Station, TX (Ocean Drilling Program), 15–55.

————, 1992b. Site 504. *In* Dick, H.J.B., Erzinger, J., Stokking, L.B., et al., *Proc. ODP, Init. Repts.,* 140: College Station, TX (Ocean Drilling Program), 37–200.

————, 1993. Site 504. *In* Alt, J.C., Kinoshita, H., Stokking, L.B., et al., *Proc. ODP, Init. Repts.,* 148: College Station, TX (Ocean Drilling Program), 27–121.

Sperkach, V.S., and Shakhpanorov, M.I., 1981. Theory of the viscosity of liquids, V. Mechanism of the viscosity of water. *Russ. J. Phys. Chem.* (Engl. Transl.), 55:981–984.

Talibudeen, O., 1981. Cation exchange in soil. *In* Greenland, D.J., and Hayes, M.H.B. (Eds.), *The Chemistry of Soil Processes:* New York (Wiley), 115–177.

Ucok, H., 1979. Temperature dependence of the electrical resistivity of aqueous salt solutions and solution-saturated porous rocks [Ph.D. thesis]. Univ. Southern California, Los Angeles.

Waxman, M.H., and Smits, L.J.M., 1968. Electrical conductivities in oil-bearing shaly sands. *SPEJ, Soc. Pet. Eng. J.,* 8:107–122.

Wilkens, R., Schultz, D., and Carlson, R., 1989. Relationship of resistivity, velocity, and porosity for basalts from downhole well-logging measurements in Hole 418A. *In* Salisbury, M.H., Scott, J.H., et al., *Proc. ODP, Sci. Results,* 102: College Station, IX (Ocean Drilling Program), 69–75.

Winsauer, W.O., and McCardell, W.M., 1953. Ionic double-layer conductivity in reservoir rocks. *Trans. AIME,* 198:129–134.

Yariv, S., and Cross, H., 1979. *Geochemistry of Colloid Systems for Earth Scientists:* New York (Springer).

Date of initial receipt: 22 August 1994
Date of acceptance: 14 March 1995
Ms 148SR-157